21st Australasian Fluid Mechanics Conference
Adelaide, Australia
10-13 December 2018

Instability of a Compliant Channel Conveying Steady and Pulsatile Turbulent Flows

K. Tsigklifis[1] **and A. D. Lucey** [1]

[1]Fluid Dynamics Research Group
Department of Mechanical Engineering
Curtin University,Perth, Westrn Australia 6845, Australia

Abstract

We investigate the stability of the fluid-structure interaction (FSI) of fully-developed steady and pulsatile turbulent mean flows through a compliant channel having flexible-plate-spring type walls. Our objective is to determine the stability maps for the onset of flow-induced flexible-wall-based instabilities that may occur in steady and pulsatile flow (at a relatively low Womersley number, $Wo = 5$) and assess the effect of structural damping on these instabilities. The mean flow of the steady and pulsatile fully-developed turbulent channel flow is modelled through the unsteady RANS equations using the Boussinesq hypothesis for the Reynolds stresses with the eddy viscosity calculated by solving the standard one-equation Spalart-Allmaras model. A spatial stability analysis is performed for steady turbulent compliant-channel flow with the extraction of the eigenvalues of the generalised eigenvalue problem for the organized disturbances, while a time-stepping procedure is devised for the calculation of the eigenvalues of the Monodromy matrix (Floquet multipliers) for the stability of the turbulent pulsatile flow. Two types of compliant-wall instability, namely a 'non-classical' travelling-wave flutter (TWF) and Divergence, that occur in both steady and pulsatile turbulent flows are identified and characterised. For lightly-damped walls, TWF yields the critical Reynolds number at which the FSI system becomes linearly unstable. It is also shown that the Stokes layer in pulsatile flow has a destabilising effect on both the TWF and Divergence instabilities with its effect on the latter being much greater.

Introduction

Much theoretical work has been done on the stability of potential [1] and viscous laminar steady [2] and pulsatile flows [3] through a flexible channel but less work has focused on the effect of steady and pulsatile time-averaged turbulent flows on the different flow-induced flexible-wall-based instabilities. The different regimes represented by the foregoing flow models have significant biomedical and microfluidic applications ranging from flows through the arteries to lab-on-a-chip technology. To extend this range of applications through the present work, we study the time-asymptotic stability of fully developed turbulent steady and pulsatile channel flows with a focus on mapping the different instability branches arising from sinuous (symmetric) modes, and the effects of mean-flow modulation and structural damping on these as well as identifying the disturbance characteristics during the modulation cycle.

System Modelling

When the pulsatile flow is turbulent, perturbations to the unsteady mean flow comprise both organised wave disturbances and turbulent fluctuations. It is the effect of the former that we study and therefore employ Reynolds averaged forms of the Navier-Stokes equations (RANS) wherein the turbulent Reynolds stresses contribute to both the determination of the mean flow and the evolution of the organised disturbances.

Mean Flow Field

We consider plane pulsatile viscous flow between two compliant walls separated by $2L^*$ distance as shown in figure 1. The characteristic length scale is chosen to be the half distance L^* between the (undisplaced) compliant surfaces, the velocity scale is the average velocity, U_B^*, of the underlying steady fully-developed turbulent channel flow about which pulsations occur, while the angular frequency of the applied periodic pulses defines the time scale, $1/\omega_f^*$. The flow field is then characterized by the Reynolds number based on the average velocity, $\mathrm{Re_B} = U_B^* L^*/\nu_l^*$, where ν_l^* is the kinematic viscosity of the fluid, and the Womersley number, $\mathrm{Wo} = L^*(\omega_f^*/\nu_l^*)^{1/2}$. Here and hereafter, * denotes a dimensional quantity.

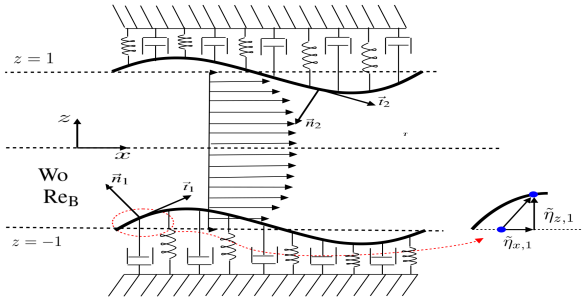

Figure 1: Schematic of the system studied

Following [4], we decompose the instantaneous velocity and pressure fields (non-dimensionlised by the dynamic pressure based on average flow velocity) as

$$u_i = \overline{u}_i + \tilde{u}_i + u_i'$$
$$p = \overline{p} + \tilde{p} + p', \tag{1}$$

with $\overline{u}_i$ and $\overline{p}$ the mean velocity and pressure, u_i' and p' the turbulent velocity and pressure fluctuations, and $\tilde{u}_i$ and $\tilde{p}$ the velocity and pressure of the organised disturbances with properties $\overline{\tilde{p}} = \overline{p'} = \overline{\tilde{u}_i} = \overline{u_i'} = 0$, $\partial\overline{u}_i/\partial x_i = \partial\tilde{u}_i/\partial x_i = \partial u_i'/\partial x_i = 0$. Then, the time average of the Navier–Stokes equations in dimensionless form are

$$\frac{\mathrm{Wo}^2}{\mathrm{Re_B}}\frac{\partial\overline{u}_i}{\partial t} + \overline{u}_j\frac{\partial\overline{u}_i}{\partial x_j} = -\frac{\partial\overline{p}}{\partial x_i} + \frac{1}{\mathrm{Re_B}}\frac{\partial^2\overline{u}_i}{\partial x_j\partial x_j} - \frac{\partial(\overline{u_i'u_j'})}{\partial x_j}, \tag{2}$$

where it has been assumed that $|\tilde{u}_i\tilde{u}_j| \ll |u_i'u_j'|$, thus $\overline{\tilde{u}_i\tilde{u}_j} \approx 0$.

In the two-dimensional system as notated in figure 1, $x_1 = x$, $x_2 = z$, $u_1 = u_x$ and $u_2 = u_z$, the mean flow is entirely in the streamwise direction x due to a mean pressure gradient in this direction and this is changed periodically with a frequency ω_f^* and amplitude Λ_T following

$$\frac{\partial\overline{p}}{\partial x} = \left.\frac{\mathrm{d}\overline{p}}{\mathrm{d}x}\right|_{st.}\left[1 + \Lambda_\mathrm{T}\frac{\exp(\mathrm{i}t) + \exp(-\mathrm{i}t)}{2}\right], \left.\frac{\mathrm{d}\overline{p}}{\mathrm{d}x}\right|_{st.} = -\frac{\mathrm{Re}_\tau{}^2}{\mathrm{Re_B}{}^2}, \tag{3}$$

with $\mathrm{Re}_\tau = \sqrt{\tau_w^*/\rho_l^*}L^*/\nu_l^*$ being the friction Reynolds number and τ_w^*, ρ_l^* the wall shear stress and the fluid density, respectively.

The closure problem for the Reynolds stresses in equation (2) is modeled via the isotropic eddy-viscosity model:

$$-\overline{u_i' u_j'} = \frac{\mathrm{G}}{\mathrm{Re_B}}\left(\frac{\partial \overline{u}_i}{\partial x_j} + \frac{\partial \overline{u}_j}{\partial x_i}\right), \tag{4}$$

with $\mathrm{G} = \nu_\tau^*/\nu_l^*$ being the dimensionless kinematic eddy viscosity.

Upon application of equation (4) in equation (2) and assuming that the axial derivatives of the Reynolds stresses due to turbulent fluctuations are small compared with their transverse counterparts, we obtain the equation that determines the mean turbulent pulsatile channel flow,

$$\frac{\mathrm{Wo}^2}{\mathrm{Re_B}}\frac{\partial \overline{u}_x}{\partial t} = -\frac{\partial \overline{p}}{\partial x} + \frac{1}{\mathrm{Re_B}}\frac{\partial^2 \overline{u}_x}{\partial z^2} + \frac{\mathrm{G}}{\mathrm{Re_B}}\frac{\partial^2 \overline{u}_x}{\partial z^2} + \frac{1}{\mathrm{Re_B}}\frac{\partial \mathrm{G}}{\partial z}\frac{\partial \overline{u}_x}{\partial z}, \tag{5}$$

with the no-slip condition, $\overline{u}_x = 0$, on the walls. The dimensionless kinematic eddy viscosity G is modelled via the "standard" one equation of Spalart-Allmaras [5] and together with the Equation (5) are solved using the Chebyshev pseudospectral method for the direction perpendicular to the mean flow using a second-order backward-difference time-stepping scheme.

Field of Organised Disturbances

We proceed by using the decomposition of (1) in the Navier-Stokes equations and applying ensemble averaging, taking into account that $\langle u_i \rangle = \overline{u}_i + \tilde{u}_i$ and $\langle p \rangle = \overline{p} + \tilde{p}$ and subtracting equation (2), obtain the equation for the organised disturbances,

$$\frac{\mathrm{Wo}^2}{\mathrm{Re_B}}\frac{\partial \tilde{u}_i}{\partial t} + \overline{u}_j\frac{\partial \tilde{u}_i}{\partial x_j} + \tilde{u}_j\frac{\partial \overline{u}_i}{\partial x_j} = -\frac{\partial \tilde{p}}{\partial x_i} + \frac{1}{\mathrm{Re_B}}\frac{\partial^2 \tilde{u}_i}{\partial x_j \partial x_j} + \frac{\partial \tilde{r}_{ij}}{\partial x_j}, \tag{6}$$

where $\tilde{r}_{ij} = -(\langle u_i' u_j' \rangle - \overline{u_i' u_j'})$ is the effect of the turbulent Reynolds stresses on the evolution of the organised disturbances and is of order $\tilde{r}_{ij} \sim O(\tilde{u}_i)$. The closure problem for $\tilde{r}_{ij}$ in equation (6) is modeled via the isotropic eddy-viscosity model that is identical to equation (4), if the mean velocities are replaced by the corresponding organised disturbance velocities.

Considering only two-dimensional organised disturbances, assuming that the field of the organised disturbances takes the spatial waveforms, $\tilde{u}_i(x,z,t) = \hat{u}_i(z,t)\exp(\mathrm{i}\alpha x) + \mathrm{c.c.}$ and $\tilde{p}(x,z,t) = \hat{p}(z,t)\exp(\mathrm{i}\alpha x) + \mathrm{c.c.}$, where α the disturbance wavenumber and substituting these in equations (6), eliminating the pressure disturbance amplitude, $\hat{p}(z,t)$, we obtain the time-dependent Orr-Sommerfeld equation which describes the evolution of the organised disturbances,

$$\begin{aligned}\mathrm{Wo}^2\frac{\partial}{\partial t}\mathcal{L}\hat{u}_z &= (\mathcal{L} - \mathrm{i}\alpha\mathrm{Re_B}\overline{u}_x)\mathcal{L}\hat{u}_z + \mathrm{i}\alpha\mathrm{Re_B}\frac{\partial^2 \overline{u}_x}{\partial z^2}\hat{u}_z \\ &\quad + \mathrm{G}\mathcal{L}^2\hat{u}_z + \frac{\partial^2 \mathrm{G}}{\partial z^2}Q\hat{u}_z + 2\frac{\partial \mathrm{G}}{\partial z}\mathcal{L}\frac{\partial \hat{u}_z}{\partial z},\end{aligned} \tag{7}$$

where $\mathcal{L} = \partial^2/\partial z^2 - \alpha^2$, $Q = \partial^2/\partial z^2 + \alpha^2$.

For the compliant-wall dynamics, we use the one-dimensional isotropic Kirchhoff plate equation with additional terms to account for a dashpot-type damping and a uniformly distributed spring foundation. Combined with the normal and tangential force balance on the two compliant walls, we obtain for the vertical and axial degrees of freedom, respectively

$$\begin{aligned}-\tilde{p}(x,z=\mp1,t) + \frac{2}{\mathrm{Re_B}}\frac{\partial \tilde{u}_z}{\partial z}(x,z=\mp1,t) \mp \frac{2}{\mathrm{Re_B}}\frac{\partial \overline{u}_x}{\partial z}(x,z=\mp1,t)\frac{\partial \tilde{\eta}_{z,s}}{\partial x} \\ = \mathrm{M_s}\frac{\partial^2 \tilde{\eta}_{z,s}}{\partial t^2} + \mathrm{D_{z,s}}\frac{\partial \tilde{\eta}_{z,s}}{\partial t} + \mathrm{K_s}\tilde{\eta}_{z,s} + \mathrm{B_s}\frac{\partial^4 \tilde{\eta}_{z,s}}{\partial x^4},\end{aligned} \tag{8}$$

$$\begin{aligned}\pm\frac{1}{\mathrm{Re_B}}\left(\frac{\partial \tilde{u}_z}{\partial x}(x,z=\mp1,t) + \frac{\partial \tilde{u}_x}{\partial z}(x,z=\mp1,t)\right) \\ = \mathrm{M_s}\frac{\partial^2 \tilde{\eta}_{x,s}}{\partial t^2} + \mathrm{D_{x,s}}\frac{\partial \tilde{\eta}_{x,s}}{\partial t} - \mathrm{A_s}\frac{\partial^2 \tilde{\eta}_{x,s}}{\partial x^2},\end{aligned} \tag{9}$$

where $\tilde{\eta}_{z,s}(x,t)$, $\tilde{\eta}_{x,s}(x,t)$ are the vertical and axial displacements of the two compliant surfaces (s=1,2 lower/upper surfaces) and $-\tilde{p}(x,z=\mp1,t)$ is the non-dimensional pressure disturbance on the compliant walls. $\mathrm{K_s}, \mathrm{B_s}, \mathrm{M_s}, \mathrm{A_s}, \mathrm{D_{z,s}}, \mathrm{D_{x,s}}$ are respectively the dimensionless spring-foundation stiffness, flexural rigidity, wall inertia, in-plane stiffness and structural damping of the walls in the vertical and axial direction, respectively, made dimensionless through the average velocity of the steady turbulent channel flow, U_B^*, the half channel height, L^* and the kinematic viscosity of the fluid, ν_l^*. Finally, the characteristic time-scale for the case of steady turbulent flow is defined through the half distance between the two plates and the average velocity of the turbulent flow ($t_{char}^* = L^*/U_B^*$).

Using the spatial wavetype decompositions $\tilde{\eta}_{z,s}(x,t) = \hat{\eta}_{z,s}(t)\exp(\mathrm{i}\alpha x) + \mathrm{c.c.}$, $\tilde{\eta}_{x,s}(x,t) = \hat{\eta}_{x,s}(t)\exp(\mathrm{i}\alpha x) + \mathrm{c.c.}$, the system of Eqs. (7) with the boundary conditions Eqs. (8), (9) and the enforcement of continuity of both the linearised tangential and vertical disturbance velocities between fluid and solid [3], is cast in the form of the following initial value problem,

$$\frac{d\vec{\hat{v}}}{dt} = \underline{\underline{Q}}(t)\vec{\hat{v}}, \quad \vec{\hat{v}} = \{\hat{c}_{z,s}, \hat{\eta}_{z,s}, \hat{c}_{x,s}, \hat{\eta}_{x,s}, \vec{\hat{u}}_x^T, \vec{\hat{u}}_z^T\}^T, \quad \vec{\hat{v}}(t=0) = \vec{\hat{v}}^0, \tag{10}$$

where $\hat{c}_{z,s} = \mathrm{d}\hat{\eta}_{z,s}/\mathrm{d}t$, $\hat{c}_{x,s} = \mathrm{d}\hat{\eta}_{x,s}/\mathrm{d}t$ and $\underline{\underline{Q}}(t)$ is periodic in time with fundamental period T, due to the imposed periodic mean velocity $\overline{u}_x$. The time-asymptotic stability of the pulsatile turbulent channel flow is then studied through the extraction of the eigenvalues (Floquet multipliers) of the monodromy matrix calculated from the fundamental solution matrix at the end of the fundamental period of mean-flow modulation [3]. Finally, the spatial asymptotic stability of the boundary-value type steady turbulent channel flow is studied through the α eigenvalue extraction of the generalized eigenvalue problem in which all perturbed quantities take the exponential form $\exp(\mathrm{i}(\alpha x - \omega_\mathrm{r} t))$, with α and ω_r being the complex wavenumber and the given real wavefrequency, respectively.

The dynamics for a 1 degree of freedom (DOF) vertical-displacement model (V) can be characterised by the dimensionless free-wave speed of the vertical due to vertical deformations, $\mathrm{C_V} = (4\mathrm{K_s B_s})^{1/4}/\mathrm{M_s}^{1/2}$. Parametrisation of the 2-DOF axial-vertical displacement model (AV) used herein additionally includes the ratio of the vertical to axial free-wave dynamics, $\mathrm{R_{VA}} = \mathrm{C_V}/\mathrm{C_A}$, where $\mathrm{C_A} = (\mathrm{A_s}/\mathrm{M_s})^{1/2}$ is the dimensionless free-wave speed of axial motion.

Results and Discussion

We first present the stability characteristics and wave phenomena that occur in steady turbulent channel derived by the spatial stability analysis for sinuous modes. In figure 2, we plot the dispersion diagrams that show the variation of complex wavenumber ($\alpha_\mathrm{i} + \mathrm{i}\alpha_\mathrm{r}$) for increasing (real) wavefrequency ω_r (indicated by the direction of the black arrows for each of the branch families) at the two values of critical $\mathrm{Re_B}$ associated with the onset of TWF and Divergence respectively. In addition, hydrodynamic and vertical-displacement structural-mode branches are also shown but the structural axial modes are omitted, because their contribution to instabilities in high Reynolds number FSI systems is small [3] for steady flows.

Without performing a rigorous causal analysis, it can be shown [6] that modes originating (for $\omega_\mathrm{i} > 0$ above the maximum temporal amplification rate) from the upper(lower) half of the α-plane are located downstream(upstream) of a notional disturbance source (wave-driver). For $\omega_\mathrm{i} = 0$, modes which appear in the right(left) half α-plane are downstream(upstream) propagating waves, respectively and modes which appear in the upper(lower) half of the α-plane are downstream stable(unstable).

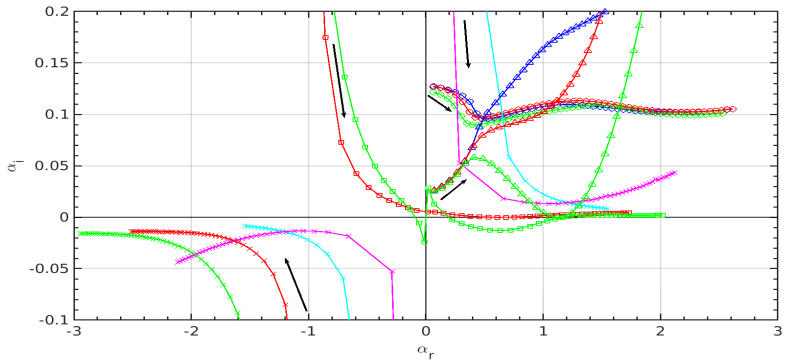

Figure 2: Dispersion diagrams of steady turbulent flow showing the variation of complex wavenumber α, for increasing real wave frequency (the direction of black arrows). Markers (⊸,⊟,⧋,✳) correspond to hydrodynamic, TWF, Divergence and structural-mode branches, respectively. Blue and red markers correspond to rigid and compliant wall cases respectively at $Re_B = 8555$ (onset of TWF instability) and green markers at $Re_B = 11901$ (onset of Divergence instability). The cyan markers correspond to the dispersion curves for the free waves of the compliant walls for vertical displacements and the magenta markers to the structural modes at almost zero mean-flow velocity ($U_B^* \approx 0.009$ m/s, $Re_B = 8555$). The axial modes are omitted. Wall parameters: $C_V = 15180$, $R_{VA} = 0.12$, $d = 1\%$.

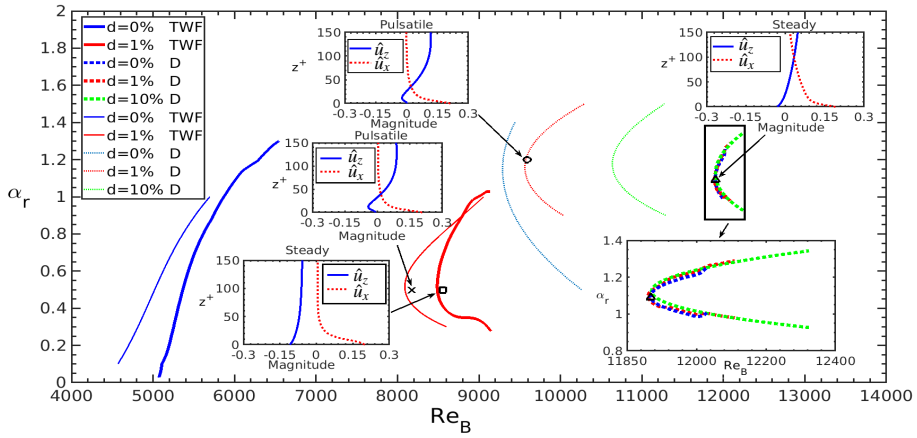

Figure 3: Neutral-stability curves from spatial-stability analysis (using Bulk Reynolds number, Re_B) for sinuous TWF and Divergence(D) instabilities, for different percentages (of critical) structural damping, for steady (thick lines) and pulsatile (thin lines) fully-developed turbulent flow through a compliant channel. Inset figures depict the corresponding normalised real part of the organised disturbance velocity eigenmodes for the steady and the pulsatile turbulent flow, respectively, as well as a zoom on the region of Divergence-instability onset for steady turbulent flow. Pulsatile flow characteristics: $Wo = 5$, $\Lambda_T = 0.872$. Wall parameters: $C_V = 15180$, $R_{VA} = 0.12$.

We first comment upon the hydrodynamic modes in figure 2 (⊸lines) that occur in both rigid- and compliant-channel flows. These modes are located downstream of the wave-driver (determined by considering $\omega_i > 0$), are downstream propagating and downstream stable for the entire range of wave frequencies ω_r. Wall compliance does little to modify the corresponding rigid-channel eigenmode shapes (not shown).

We now focus on the TWF instability that is marginally unstable at $Re_B = 8555$ in figure 2. The TWF mode branch (⊟line) indicates that these modes are located downstream of the wave-driver and are upstream propagating and downstream stable for $\omega_r' < 0.886$ ($t^*_{char} = L^*/U_B^*$) or $\omega_r < 303$ ($t^*_{char} = 1/\omega_f^*$, for $Wo = 5$). For higher frequencies they change their direction to downstream propagating and downstream stable except at the critical frequency $\omega_r' \approx 1.328$ ($\omega_r \approx 455$) where the TWF mode become downstream unstable. At the higher $Re_B = 11901$ (green line) there is seen a range of downstream propagating, unstable wavenumbers over a finite range of wave frequencies. We term these 'non-classical' TWF instabilities because they are fast waves with wavespeed $c = c^*/U_B^* > 1$ whereas classical TWF (e.g. see [6]) has $c < 1$. The present instability is very sensitive to structural damping (critical $Re_B = 5068$ with $c \approx 53$ for $d = 0$ rising to critical $Re_B = 8555$ with $c \approx 2.2$ for $d = 1\%$, where $d = D_{z,s}/(2\sqrt{M_s K_s})$ is the structural damping relative to its critical value). This type of instability also exists for inviscid flow through flexible channels [7]. These TWF branches originate from the downstream propagating downstream stable in-vacuo structural vertical displacement modes and their counterparts with fluid inertia (✳lines). It is the mean-flow fluid loading that increasingly modifies their wave characteristics as Re_B is increased in figure 2 leading to the onset of unstable behaviour.

The instability termed Divergence herein is different to that encountered in open flows (e.g. see [8]) because it is caused by bulk motions of the fluid within the core of the channel. Thus, the divergence-mode branch (⧋lines) exists in turbulent flow through a rigid channel (blue line) with modes located downstream of the wave-driver and characterised as downstream propagating, downstream stable. When wall compliance is introduced this branch become less stable and when the fluid-flow loading is increased sufficiently to that at $Re_B = 11901$, instability-onset occurs with waves being downstream unstable at $\omega_r' \approx 0.906$ ($\omega_r \approx 431$) with wave speed $c \approx 0.83$.

Finally in figure 2 we remark that the vertical structural modes (✳lines) in the left half α-plane are located upstream of the wave driver, upstream propagating and are downstream unstable modes (or, equivalently, stable in their direction of propagation).

From results such as those presented in figure 2, the neutral-stability diagram of figure 3 is generated that indicates the values of bulk Reynolds number Re_B, at which instability onset occurs for each of sinuous TWF and Divergence instabilities. The results also include the effect of structural damping (as a

percentage of critical damping). It is seen that Pulsatile turbulent flow is less stable for sinuous channel-wall deformations in TWF (identified by the first unstable Floquet multiplier) and Divergence instabilities (identified by the second unstable multiplier) than the underlying (i.e. zero pulsation) steady turbulent flow. In addition, structural damping is seen to have a strong stabilizing effect on the TWF and Divergence instabilities in pulsatile turbulent flow and an equally stabilizing effect on the TWF in steady turbulent flow, while it has almost negligible effect on Divergence due to steady turbulent flow (see inset figure for detail). The action of structural damping decreases the wavelength of the most unstable TWF mode, while that of the most unstable Divergence mode remains almost unaffected in both the steady and pulsatile turbulent flows. Finally, it is seen that, for the low levels of structural damping used to generate figure 3, TWF yields the critical $\mathrm{Re_B}$; however, higher levels of damping that increasingly stabilise TWF will cause divergence to become the critical instability.

The insets in figure 3 show the eigenmodes at the minimum $\mathrm{Re_B}$ of each branch. For both steady and pulsatile flows the TWF instability has higher gradient of disturbance velocities at the wall than those of Divergence. In addition, the TWF and Divergence instabilities in the pulsatile flow exhibit higher gradients than those of the corresponding instabilities in steady turbulent flow. The associated increase of disturbance shear stresses on the wall for sinuous Divergence instability in the pulsatile flow and the concomitant large reduction of the critical $\mathrm{Re_B}$ of the instability, is attributed to the action of the Stokes layer. The thickness of the laminar Stokes layer in wall units is $\delta^+ = \sqrt{2}\mathrm{Re}_\tau/\mathrm{Wo} \approx 148$ and it therefore penetrates the whole inner part of the turbulent boundary layer. It therefore appears that flow pulsation disrupts the effect of the laminar sub-layer in isolating the compliant wall from the fluid motions within the core of the channel that occurs for steady flow and this results in lower values of critical $\mathrm{Re_B}$. By contrast, the Stokes layer is seen to have only a small destabilising effect on the TWF-instability mechanism.

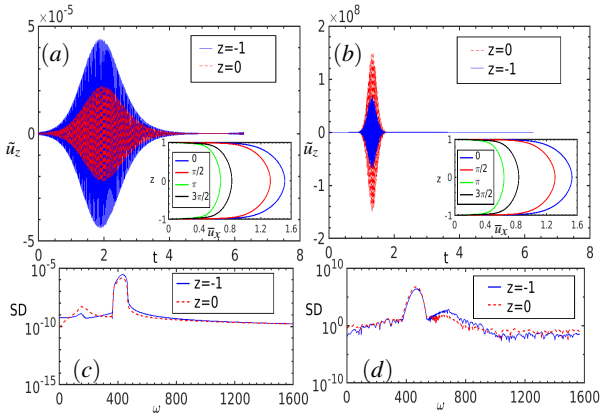

Figure 4: Time evolution of $\tilde{u}_z$ during one period of pulsation and corresponding spectral density at the bottom compliant wall (blue line) and at the channel centreline (red line) for the pulsatile fully-developed turbulent flow (a) & (c) at TWF instability onset ($\mathrm{Re_B} = 8171, \alpha_r = 0.5$), (b) & (d) at Divergence instability onset ($\mathrm{Re_B} = 9588, \alpha_r = 1.2$). Inset figures depict the corresponding pulsatile mean flow velocity profiles. Pulsatile flow characteristics: $\mathrm{Wo} = 5$, $\Lambda_T = 0.872$. Wall parameters: $C_V = 15180$, $R_{VA} = 0.12$, $d = 1\%$.

In order to reveal the characteristics of the FSI during the pulsation cycle, we plot in figures 4(a) and (b) the time evolution of the vertical disturbance velocity at the channel centreline and at the bottom wall during one period of pulsation of the mean flow depicted in the inset figures, for the cases of the TWF and Divergence onset (respectively the cross and circle markers in figure 3). In both cases, the amplitude of the oscillations increase at the beginning of the deceleration phase of the pulsatile mean flow just after the mean velocity profile acquires a maximum. For TWF, the amplitudes of oscillation are larger on the wall relative to those at the channel centreline, an indication of a wall mode instability. However, for Divergence instability the oscillation amplitude at the channel centreline is larger than that at the wall; this reinforces the discussions of figures 2 and 3 that pointed to it being principally caused by fluid motions within the core of the channel.

Figures 4(c) and (d), show the corresponding spectral densities of figures (a) and (b). Two local maxima appear in each figure. For the TWF instability-onset case, (c), one maximum appears at $\omega \approx 433$ and one at $\omega \approx 153$, the first corresponding to the frequency of the TWF instability, also in agreement with that predicted for the steady turbulent flow, while the latter is associated with the hydrodynamic mode with $\alpha_r = 0.5$. Similar conclusions hold for the Divergence instability, (d), but here the spectrum appears broader with the maximum peaks at $\omega \approx 467$ and $\omega \approx 683$, respectively.

Conclusions

We have studied the time asymptotic stability of steady and pulsatile turbulent flows through a compliant channel considering the sinuous modes of disturbance oscillations. We identified the TWF and Divergence instability branches which appear as downstream travelling, downstream amplified, modes in steady turbulent channel flow. The TWF instability appears as a 'non-classical', very fast, mode that is very sensitive to structural damping mode while its branch form is similar to that of flexible channels conveying potential flow, [7]. Flow pulsation is destabilising, relative to the corresponding steady flow, for both the TWF and Divergence instabilities with the effect on the latter being much greater. For low levels of structural damping, TWF-onset yields the critical Reynolds number but Divergence may become the critical instability with high levels of structural damping.

References

[1] Burke, M.A., Lucey, A.D., Howell, R.M. and Elliott, N. S.J., Stability of a flexible insert in one wall of an inviscid channel flow. *Journal of Fluids and Structures*, **48**, 2014, 435–450.

[2] Davies, C. and Carpenter, P.W., Instabilities in a plane channel flow between compliant walls. *Journal of Fluid Mechanics*, **352**, 1997, 205–243.

[3] Tsigklifis, K. and Lucey, A.D., Asymptotic stability and transient growth in pulsatile Poiseuille flow through a compliant channel, *Journal of Fluid Mechanics*, **820**, 2017, 370–399.

[4] Sen, P.K. and Veeravalli, S.V., On the Behaviour of Organised Disturbances in a Turbulent Boundary-Layer, *Sadhana*, **23**, 2, 1998, 167–193.

[5] Spalart, P.R. and Allmaras, S.R., A One-Equation Turbulence Model for Aerodynamic Flows, *Recherche Aerospatiale*, **1**, 1994, 5–21.

[6] Ashpis, D.E. and Reshotko, E., The vibrating ribbon problem revisited, *Journal of Fluid Mechanics*, **213**, 1990, 531–547.

[7] De Langre, E. and Ouvrard, A.E., Absolute and convective bending instabilities in fluid-conveying pipes, *Journal of Fluids and Structures*, **13**, 1999, 663–680.

[8] Tsigklifis, K. and Lucey, A.D., The interaction of Blasius boundary-layer flow with a compliant panel: global, local and transient analyses, *Journal of Fluid Mechanics*, **827**, 2017, 155–193.